Engineering Structures 292 (2023) 116498

Contents lists available at ScienceDirect

Engineering Structures

journal homepage: www.elsevier.com/locate/engstruct

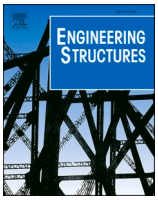

Bridge topology optimization considering stochastic moving traffic

Thomas Golecki [a,*], Fernando Gomez [b], Juan Carrion [c,d], Billie F. Spencer Jr [a]

[a] Civil and Environmental Engineering, University of Illinois at Urbana–Champaign, 205 N Mathews Ave, Urbana, 61801, IL, USA
[b] College of Science and Engineering, Universidad San Francisco de Quito, Diego de Robles y Via Interoceanica, Quito, Ecuador
[c] Skidmore, Owings & Merrill, LLP, 224 S Michigan Ave #1000, Chicago IL, 60604, IL, USA
[d] Department of Civil Engineering, University of Cuenca, Cuenca, Ecuador

ARTICLE INFO

Keywords:
Topology optimization
Stochastic dynamics
Random traffic loading
Lyapunov equation

ABSTRACT

Topology optimization of bridge structures is challenging due to the difficulty in accounting for the stochastic dynamic nature of the moving vehicle loads. As a result, optimization for this common type of structure and loading is limited in the existing literature. Existing topology optimization approaches for addressing stochastic dynamic loading can be classified as time domain, frequency domain, or random vibration methods. Herein, a new compact representation of random moving traffic loading as a filtered white noise is developed which enables stochastic topology optimization to be performed. This optimization utilizes an objective function which combines the mean and standard deviation of responses to minimize the extreme response to random traffic loading. Examples show a significant improvement of the bridge response, represented by a reduction in the standard deviation at a minimal cost to the mean response. Also, optimal topologies for different traffic parameters such as speed and arrival rate are relatively similar, indicating a robust solution. With this approach, bridge topology can be efficiently optimized for random moving traffic loading by enabling direct minimization of response extremes, which represents the probabilistic design intent to achieve adequate levels of performance under the loading uncertainties in typical bridges.

1. Introduction

The importance of transportation infrastructure cannot be overstated. In both rail lines and highways, bridges are a critical component of the transportation network, not only for crossing natural obstacles, but also other infrastructure. In the United States alone, there have been an average of more than 50,000 new roadway bridges built each decade since 1950 [1]. The constant need for new bridge construction presents an opportunity to extend recent developments in structural optimization to enable more efficient structural systems, while still meeting design objectives. A major challenge here is that modern bridge design codes aim for a uniform level of reliability by accounting for intrinsic uncertainty. This reliability is achieved by applying calibrated load and resistance factors to the design load and nominal resistance. These factored loads simulate the upper tail of the probabilistic load, i.e., mean plus a number of standard deviations. However, accounting for this loading uncertainty in structural optimization is challenging.

Some researchers have used topology optimization to investigate the influence of various conditions on optimal bridge design. For example, multiple authors considered self-weight [2–4], member buckling [5–7], or multiple materials [8–10] in the optimization formulation. Other researchers examined different tension and compression behavior [9,11–14], constructability [15], and aesthetics [16–18]. In these papers, traffic is represented as a uniform static load. Other researchers have explicitly modeled the traffic loading as a discrete random field load [19–22], where loading consists of static point loads of random magnitude and location, or a continuous random field load [23–26], where loading is represented by a static distributed load with random amplitude. Alternatively, dynamic traffic loading can be modeled as a deterministic moving load. Giraldo-Londoño and Paulino [27] developed a topology optimization that could account for deterministic dynamic loads and provided an example for a bridge structure. All of these studies approximate the traffic loading as static and or deterministic, neglecting the random dynamic nature of these loads.

Very little research has appeared regarding topology optimization of structures subjected to stochastic dynamic loads. Some work has been done for wind and earthquake loaded structures [28,29], which assume that the loading is a continuous random process. Because traffic loading is a discrete random field process, direct application of this approach to topology optimization of bridge structures subjected to traffic loading is

* Corresponding author.
E-mail address: golecki2@illinois.edu (T. Golecki).

https://doi.org/10.1016/j.engstruct.2023.116498
Received 9 March 2023; Received in revised form 9 June 2023; Accepted 14 June 2023
Available online 3 July 2023

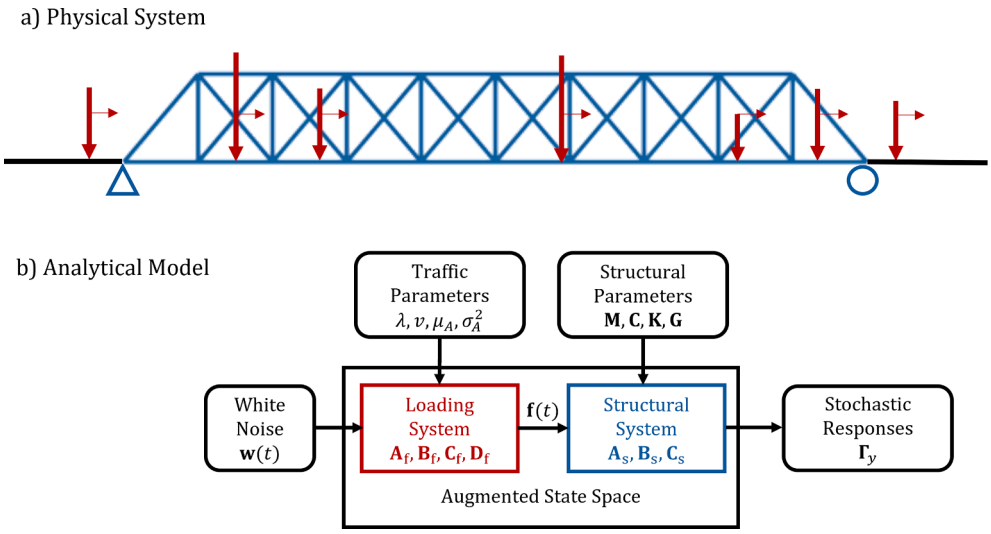

Fig. 1. a Schematic of an arbitrary bridge subjected to moving random loads (b) Block diagram interpretation of the analytical model.

not possible. Golecki et al. [30] proposed a continuous random process representation of the traffic loading and employed it for the analysis of truss-type structures. While this approach is promising, topology optimization is shown herein to require a finer discretization of the load than is currently feasible, leaving topology optimization of bridge structures due to stochastic dynamic traffic loading yet to be reported.

In this paper, an approach for bridge topology optimization that explicitly considers the stochastic dynamic nature of the traffic loading is proposed. First, a new compact formulation of the continuous random process model of the traffic loading is presented that enables efficient bridge topology optimization to be achieved. Subsequently, this stochastic topology optimization framework is adapted to allow for a reliability-based interpretation. Finally, the efficacy of the proposed approach is demonstrated through several numerical studies. This approach is intended to serve as a part of the conceptual design process. After optimization, discrete members can be interpreted from the topology in the next phase of the design allowing for engineering judgement as well as other design considerations such as aesthetics and constructability. The remainder of this paper is organized as follows. Section 2 presents the structural and loading systems represented together in an augmented state space system to enable solving for the stochastic responses. The topology optimization formulation and solution approach is discussed in Section 3 followed by a numerical example in Section 4 and conclusions in Section 5.

2. Stochastic response of bridges subjected to vehicular traffic

Consider the bridge structure shown in Fig. 1a, where the random traffic loading is a discrete random field, with vehicles represented by point loads of random weight and spacing moving at a constant speed. To determine the stochastic response of the bridge, Golecki et al. [30] proposed a continuous filtered white noise model for vehicular bridge traffic and utilized random vibration theory to determine the stochastic responses as outlined in the block diagram of Fig. 1b. For the convenience of the reader, this approach is first briefly reviewed. Then, the computational effort required in this approach is explored and shown to be intractable for structural optimization purposes. Subsequently, a new compact formulation of the traffic loading model is proposed that will enable bridge topology optimization, as formulated in Section 3.

2.1. Stochastic structural responses

The response of an arbitrary linear system can be defined via the state space representation. For this application, the augmented system shown in Fig. 1b consists of a loading system in series with a structural system. The state space representation of the filter modeling the stochastic load is given by

$$\dot{\mathbf{x}}_f = \mathbf{A}_f\mathbf{x}_f + \mathbf{B}_f\mathbf{w}(t)$$

$$\mathbf{f}(t) = \mathbf{C}_f\mathbf{x}_f \tag{1}$$

where $\mathbf{A}_f$, $\mathbf{B}_f$, and $\mathbf{C}_f$ are the system matrices, $\mathbf{w}(t)$ is a white noise input process, and $\mathbf{f}(t)$ is the vector of output forces at locations along the bridge. The state space representation of the structure is given by

$$\dot{\mathbf{x}}_s = \mathbf{A}_s\mathbf{x}_s + \mathbf{B}_s\mathbf{f}(t)$$

$$\mathbf{y} = \mathbf{C}_s\mathbf{x}_s + \mathbf{D}_s\mathbf{f}(t) \tag{2}$$

where the state vector $\mathbf{x}_s$ represents the displacement and velocity of bridge degrees of freedom (DOF), $\mathbf{f}(t)$ is the input loading vector and system matrices are defined as

$$\mathbf{A}_s = \begin{bmatrix} \mathbf{0} & \mathbf{I} \\ -\mathbf{M}^{-1}\mathbf{K} & -\mathbf{M}^{-1}\mathbf{C} \end{bmatrix}, \quad \mathbf{B}_s = \begin{bmatrix} \mathbf{0} \\ -\mathbf{M}^{-1}\mathbf{G} \end{bmatrix} \tag{3}$$

where $\mathbf{M}, \mathbf{C}, \mathbf{K}$, and $\mathbf{G}$ are the mass, damping, stiffness, and load effect matrices respectively, $\mathbf{0}$ is a matrix of zeros and $\mathbf{I}$ is an identity matrix.

The state space and measurement equations for the augmented system shown in Fig. 1b are given by

$$\dot{\mathbf{x}}_a = \mathbf{A}_a\mathbf{x}_a + \mathbf{B}_a\mathbf{w}(t)$$

$$\mathbf{y} = \mathbf{C}_a\mathbf{x}_a \tag{4}$$

where $\mathbf{A}_a$, $\mathbf{B}_a$ and $\mathbf{C}_a$ are the state space matrices of the augmented system, $\mathbf{x}_a$ is the augmented state vector, and $\mathbf{y}$ is a vector of output quantities. The augmented state space matrices are given by

$$\mathbf{A}_a = \begin{bmatrix} \mathbf{A}_s & \mathbf{B}_s\mathbf{C}_f \\ \mathbf{0} & \mathbf{A}_f \end{bmatrix} \quad \mathbf{B}_a = \begin{bmatrix} \mathbf{0} \\ \mathbf{B}_f \end{bmatrix} \tag{5}$$

$$\mathbf{C}_a = \begin{bmatrix} \mathbf{C}_s & \mathbf{D}_s\mathbf{C}_f \end{bmatrix}$$

The covariance of the response of this system to a stationary zero-mean stochastic excitation is given by the Lyapunov equation [31]

$$\mathbf{A}_a\boldsymbol{\Gamma}_x + \boldsymbol{\Gamma}_x\mathbf{A}_a^T + 2\pi\mathbf{B}_a\mathbf{S}_0\mathbf{B}_a^T = \mathbf{0}$$

$$\boldsymbol{\Gamma}_y = \mathbf{C}_a\boldsymbol{\Gamma}_x\mathbf{C}_a^T \tag{6}$$

where $\mathbf{S}_0$ is the magnitude of the two-sided constant power spectral density (PSD) of the input, and $\mathbf{\Gamma}_x$ and $\mathbf{\Gamma}_y$ are the covariance matrices of the system states and measured response, respectively. The next section describes how the random traffic loading can be represented as a filtered white noise process.

2.2. Continuous filtered white noise representation of vehicular traffic

The most common approach to modeling random traffic loads is as a spatiotemporal random field, $f(x,t)$, in which the arrival of vehicles at the bridge is defined by a compound Poisson process. The vehicles are represented as random magnitude point loads, with a mean, μ_A, and standard deviation, σ_A, arriving at random times with a constant arrival rate, λ (vehicles/time), and travel across the bridge at a constant speed, v. The corresponding traffic density (vehicles/length) is computed as λ/v. Additional traffic lanes can be represented as separate independent random processes. This process can be shown to be weakly stationary, with a static mean $\mu_f = \mu_A\lambda/v$ and a power spectral density given by

$$S(\Delta x,\omega) = \frac{\lambda\left(\mu_A^2+\sigma_A^2\right)}{2\pi v^2}e^{-i\omega\frac{\Delta x}{v}} \tag{7}$$

where Δx is the distance along the span, and ω is in radians/sec. The term $\lambda\left(\mu_A^2+\sigma_A^2\right)/2\pi v^2$ is a constant scaling factor; the complex exponential $\exp(-i\omega\Delta x/v)$ is the frequency domain representation of the time delay, $\Delta x/v$, which corresponds to the time required for the load to travel a distance Δx. Because of this time delay, creating a loading model such as is given in Eq. (1) that has the PSD given in Eq. (7) requires an infinite dimensional state space representation [32], which is not realizable. To address this problem, Golecki et al. [30] used Padé approximants, which are rational polynomial approximations of the time delay function with a polynomial order selected to ensure accuracy up to a specified target frequency. The random field for the traffic loading is then discretized in space realized into the state space representation given in Eq. (1). The interested reader is directed to Golecki et al. [30] for more information.

While effective, the accuracy of this approach is a function of the spatial discretization for the random process. Topology optimization requires a relatively fine discretization of the load, which results in very large loading system matrices. A balanced model reduction can be applied to reduce the size of the system and the associated time to compute the stochastic responses [33]; however, this balanced reduction operation can be extremely time and memory intensive. For example, balanced model reduction of a loading system with 256 outputs, $\Delta x/v = 0.03s$, and a typical target frequency of 5 Hz fails due to memory limits on a machine with 32 Gb of RAM. A new approach is required to use this traffic loading model for topology optimization.

2.3. New compact formulation of traffic loading model

This section proposes a new compact formulation of the traffic loading model that increases computational efficiency and enables the subsequent topology optimization. The state space representation of the traffic loading system described in the previous section builds a system of delays for each point corresponding to the spatial discretization of the loading on the bridge. The state space matrix $\mathbf{A}_f$ is block diagonal, with each block representing one of the Padé approximants, which results in an extremely large and sparse matrix; the subsequent model reduction requires very large computational resources and time. To reduce the computational burden, longer delays can be represented as a combination of shorter delays, which enables the same subsystem to be used as a part of multiple spatially discretized outputs. In this approach, referred to here as the compounding method, the assembly is represented as

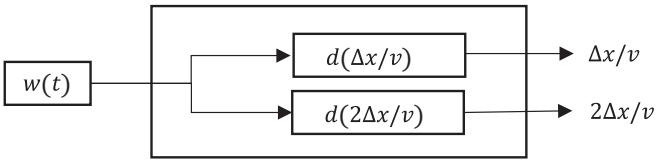

Fig. 2. Block diagram representation of the system $\boldsymbol{d}_2$, from Eq. (8) with outputs labeled with their time delay.

$$\boldsymbol{d}_2 = \begin{bmatrix} d(\Delta x/v) \\ d(2\Delta x/v) \end{bmatrix} \tag{8}$$

$$\boldsymbol{d}_{2^{i+1}} = \begin{bmatrix} \boldsymbol{d}_{2^i} \\ d\left(2^i\Delta x/v\right)*\boldsymbol{d}_{2^i} \end{bmatrix} \text{ for } i = 1, 2, \cdots \tag{9}$$

where $d(\Delta x/v)$ represents a state space system for the time delay of $\Delta x/v$, $\boldsymbol{d}_n$ represents the assembled system for all delays from $\Delta x/v$ to $n\Delta x/v$, and the operator * represents combining the two systems in series (i.e., creating a single system using the output of the first system as the input to the second). A block diagram representation of Eq. (8) is provided in Fig. 2. The assembly procedure starts with the base system in Eq. (8), then iteratively applies Eq. (9) as many times as needed for the given domain. For instance, a loading system of 512 outputs would include indices $i = 1$ through $i = 8$, where the final application of Eq. (9) would produce a system with 2^9 outputs. An example of the iterative assembly procedure including a block diagram representation at each iteration is shown in Appendix A.

This formulation of the loading system results in a substantial reduction in the overall size of the model. Fig. 3a depicts the size and sparsity of the matrix $\mathbf{A}_f$ using the approach in [30], with a spatial discretization of 128 points, and $\Delta x/v = 0.06s$. Fig. 3b shows the resulting matrix $\mathbf{A}_f$ using the new compact formulation, which is substantially smaller, although it is no longer block diagonal. The compounding method results in a 94% reduction of the number of nonzero values needed to define the system. The resulting behavior of these two system assembly approaches is shown in Fig. 3c which compares the phase angle of the outputs corresponding to the time required to travel 1/4, 1/2 and 3/4 of the span with the exact phase of $-\Delta x\omega/v$. The agreement below the 5 Hz target frequency indicates equivalent behavior of both methods. Using this new formulation, the balanced reduction operation takes much less time, less than 60 s for this system built by the compounding method, compared to 73 min for the original method. However, this spatial discretization is shown in the later examples to be inadequate for topology optimization. For a more refined spatial discretization of the loading system (e.g., 256 points), balanced reduction of the system using the original formulation failed, whereas the proposed compact formulation successfully completed in 5 min on a computer with an Intel Xeon E3- 1285 v6 @4.10 GHz processor and 32 Gb of RAM. This compact form of the loading system enables efficient balanced reduction of loading systems needed for optimization with vastly reduced computational resources.

3. Topology optimization

The topology optimization design domain is shown schematically in Fig. 4, with the temporally continuous spatially discrete representation of random traffic loading superimposed. The bridge structure described by Eqs. (2) and (3) is represented as a 2D mesh of plane stress elements. Here the density method is employed, where design variables, z, represent the individual element densities and are continuous between zero and one. Thus, the optimization statement can be given by

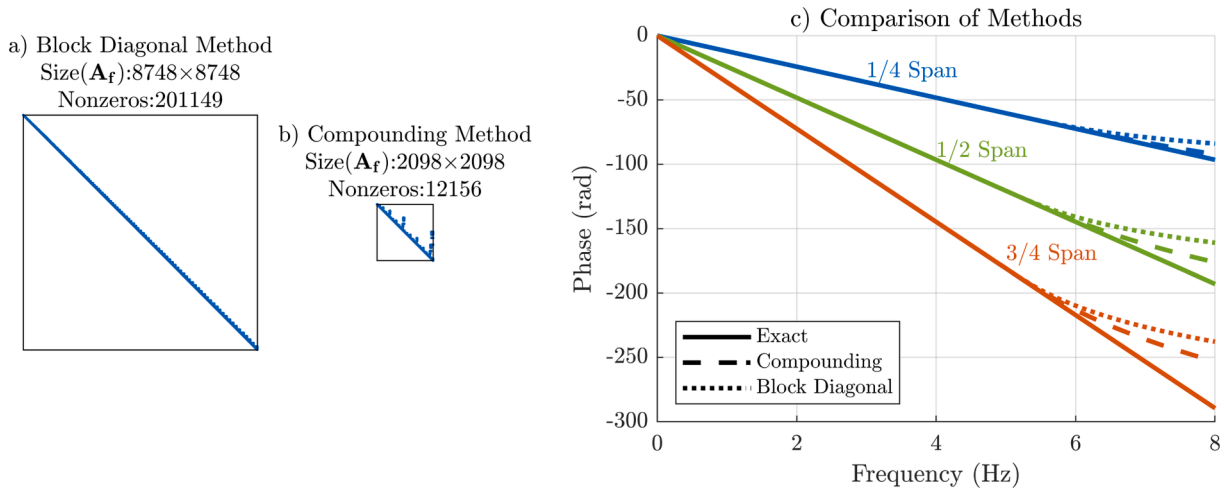

Fig. 3. Size and sparsity comparison of an example loading system matrix, $\mathbf{A}_\mathrm{f}$, built using (a) the block diagonal method and (b) the compounding method. (c) A comparison of select outputs from both methods compared to the exact value.

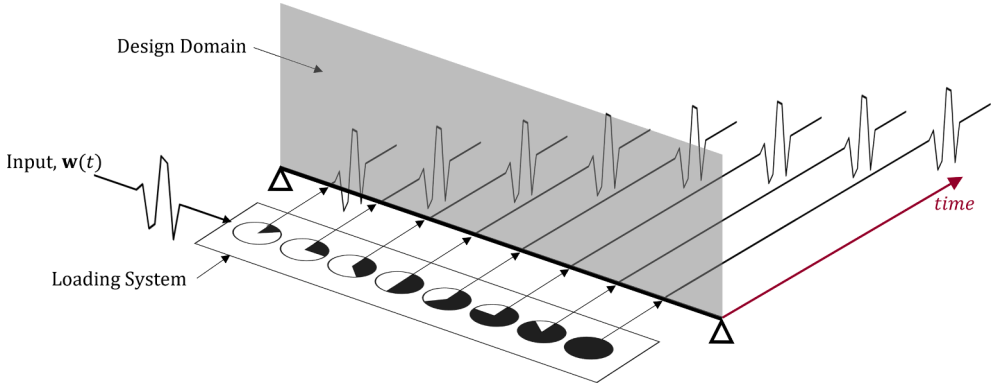

Fig. 4. Schematic of the idealized optimization problem of a bridge subjected to random moving traffic loads, where the horizontal axis normal to the structure represents time; a random input process is delayed incrementally and applied at discrete locations representing movement across the span.

$$
\begin{aligned}
\min_{z} \quad & J(z) = \phi(\mathbf{\Gamma}_\mathrm{x}(z), \boldsymbol{\mu}_\mathbf{u}(z), z) \\
\text{s.t.} \quad & g(z) = V(z) - V_{max} = 0 \\
& \mathbf{A}_\mathrm{a}\mathbf{\Gamma}_\mathrm{x} + \mathbf{\Gamma}_\mathrm{x}\mathbf{A}_\mathrm{a}^\mathrm{T} + 2\pi\mathbf{B}_\mathrm{a}\mathbf{S}_0\mathbf{B}_\mathrm{a}^\mathrm{T} = 0 \\
& \mathbf{K}\boldsymbol{\mu}_\mathbf{u} = \mathbf{G}\boldsymbol{\mu}_\mathbf{f} \\
& z_n \in [z_{min}, z_{max}] \text{ for } n = 1, 2, \ldots N_{el}
\end{aligned}
\tag{10}
$$

where the objective function $J(z)$ is a function, ϕ, of the covariances, $\mathbf{\Gamma}_\mathrm{x}(z)$, and the static mean, $\boldsymbol{\mu}_\mathbf{u}(z)$, of the stochastic dynamic responses. The total volume, $V(z)$, is constrained by V_{max}. Two state equations are considered, one for the covariances and the other for the static mean of the stochastic dynamic responses. In the static state equation, $\mathbf{K}$ is the structural stiffness matrix, $\boldsymbol{\mu}_\mathbf{f}$ is the spatially discretized vector of mean nodal loads, $\boldsymbol{\mu}_\mathbf{u}$ is the vector of displacements due to the mean loads and $\mathbf{G}$ is the load effects matrix. Design variables are limited to be between z_{min} and z_{max}; here we use bounds of 0.001 and 1.0 and N_{el} is the total number of elements in the domain.

3.1. Objective functions

Minimizing the sum of nodal responses of the vertical DOF at the floorbeam nodes is considered as the optimization objective. As those are also the loaded degrees of freedom, where each DOF experiences the same moving vehicle load, this objective is somewhat akin to a dynamic compliance objective. These output responses are selected in constructing the $\mathbf{C}_\mathrm{s}$ and $\mathbf{D}_\mathrm{s}$ matrices, which is then used in Eq. (5) to determine $\mathbf{C}_\mathrm{a}$. Because the responses of interest specified in the $\mathbf{C}_\mathrm{s}$ matrix are displacements, which have a nonzero response to the mean loading, a combined objective of the mean plus k standard deviations is proposed here, based on the design intent of reliability-based design codes, which typically scale load effects from a nominal load by calibrated load factors to represent the upper tail of the probabilistic load. Here, we achieve a similar intent by optimizing for the upper tail of the probabilistic response represented by

$$
J_{\mu k\sigma}(z) = J_\mathrm{som}(z) + kJ_\mathrm{sosd}(z) \tag{11}
$$

where k is a constant. There are two components here, first the sum of means, given by J_som, is

$$
J_\mathrm{som}(z) = \sum \mathbf{C}_\mathrm{s} \begin{bmatrix} \mathbf{K}(z)^{-1}\mathbf{G}\boldsymbol{\mu}_\mathbf{f} \\ \mathbf{0} \end{bmatrix} = \mathbf{L}_\mathrm{s}^\mathrm{T}\boldsymbol{\mu}_\mathbf{u} \tag{12}
$$

where $\mathbf{L}_\mathrm{s}$ is a vector of zeros except for ones at the DOF included in the objective. In this expression, $\boldsymbol{\mu}_\mathbf{u}$ is the vector of mean responses, which when multiplied by $\mathbf{L}_\mathrm{s}^\mathrm{T}$ results in the sum of means of selected DOF. Second, the sum of standard deviations, given by J_sosd, is

$$
J_\mathrm{sosd}(z) = \mathrm{tr}\left(\mathbf{C}_\mathrm{a}(\mathbf{\Gamma}_x(z))^{\circ\frac{1}{2}}\mathbf{C}_\mathrm{a}^\mathrm{T}\right) \tag{13}
$$

where $\circ$ is the Hadamard (elementwise) operation and $\mathrm{tr}(\bullet)$ is the trace operator. The elementwise square root converts the diagonals of the covariance matrix into standard deviations, the multiplications by $\mathbf{C}_\mathrm{a}$

removes DOF not included in the objective and the trace operator sums the remaining standard deviations.

3.2. Response sensitivities

The optimization procedure considered here is gradient-based, and therefore requires computing the sensitivities of the objective and constraint functions with respect to the design variables. As the mean loading portion of the combined objective given by J_{som} is static, this portion of the sensitivity calculation is readily available in other references [34,35] and is not derived here. This sensitivity is given by

$$\frac{\partial J_{\text{som}}}{\partial z} = \left(-\mathbf{L}_{\text{s}}^{\text{T}}\mathbf{K}^{-1}\right)\left(\frac{\partial \mathbf{K}}{\partial z}\boldsymbol{\mu}_{\mathbf{u}}\right) \tag{14}$$

The sensitivity of the sum of standard deviation objective given by J_{sosd} is computed using the adjoint method. Here, the residual is the stationary Lyapunov equation

$$\mathbf{R} = \mathbf{A}_{\text{a}}\boldsymbol{\Gamma}_{\text{x}} + \boldsymbol{\Gamma}_{\text{x}}\mathbf{A}_{\text{a}}^{\text{T}} + 2\pi\mathbf{B}_{\text{a}}\mathbf{S}_0\mathbf{B}_{\text{a}}^{\text{T}} = \mathbf{0} \tag{15}$$

and the Lagrangian including the adjoint matrix $\boldsymbol{\Lambda}$ is

$$\mathscr{L} = J_{\text{sosd}} + \text{tr}(\boldsymbol{\Lambda}\mathbf{R})$$

$$\mathscr{L} = \text{tr}\left(\mathbf{C}_{\text{a}}(\boldsymbol{\Gamma}_{\text{x}}(z))^{\circ\frac{1}{2}}\mathbf{C}_{\text{a}}^{\text{T}}\right) + \text{tr}\left(\boldsymbol{\Lambda}\left(\mathbf{A}_{\text{a}}\boldsymbol{\Gamma}_{\text{x}} + \boldsymbol{\Gamma}_{\text{x}}\mathbf{A}_{\text{a}}^{\text{T}} + 2\pi\mathbf{B}_{\text{a}}\mathbf{S}_0\mathbf{B}_{\text{a}}^{\text{T}}\right)\right) \tag{16}$$

The resulting sensitivity is

$$\frac{\partial \mathscr{L}}{\partial z} = \text{tr}\left(\frac{\partial \mathbf{C}_{\text{a}}\mathbf{C}_{\text{a}}^{\text{T}}}{\partial z}\boldsymbol{\Gamma}_{\text{x}}^{\circ\frac{1}{2}}\right) + \text{tr}\left(\left(\frac{\partial \mathbf{A}_{\text{a}}}{\partial z}\boldsymbol{\Gamma}_{\text{x}} + \boldsymbol{\Gamma}_{\text{x}}\frac{\partial \mathbf{A}_{\text{a}}^{\text{T}}}{\partial z} + \frac{\partial}{\partial z}\left(2\pi\mathbf{B}_{\text{a}}\mathbf{S}_0\mathbf{B}_{\text{a}}^{\text{T}}\right)\right)\boldsymbol{\Lambda}\right) \tag{17}$$

where the adjoint matrix $\boldsymbol{\Lambda}$ is determined by the Lyapunov equation

$$\mathbf{A}_{\text{a}}^{\text{T}}\boldsymbol{\Lambda} + \boldsymbol{\Lambda}\mathbf{A}_{\text{a}} + \frac{\phi}{\partial \boldsymbol{\Gamma}_{\text{x}}} = \mathbf{0} \tag{18}$$

For the sum of standard deviation objective function, $\phi = J_{\text{sosd}}$, the partial derivative with respect to the state variance, $\partial J_{\text{sosd}}/\partial \boldsymbol{\Gamma}_{\text{x}}$, is computed as

$$\frac{\partial J_{\text{sosd}}}{\partial \boldsymbol{\Gamma}_{\text{x}}} = \mathbf{C}_{\text{a}}\text{diag}\left(\frac{d\boldsymbol{\Gamma}_{\text{x}}^{\circ\frac{1}{2}}}{d\boldsymbol{\Gamma}_{\text{x}}}\right)\mathbf{C}_{\text{a}}^{\text{T}} = \frac{1}{2}\mathbf{C}_{\text{a}}\text{diag}\left(\boldsymbol{\Gamma}_{\text{x}}^{\circ-\frac{1}{2}}\right)\mathbf{C}_{\text{a}}^{\text{T}} \tag{19}$$

Where $\text{diag}(\bullet)$ represents the diagonal operator, with only the diagonal elements of the matrix. Note that the elementwise square root does not necessarily preserve the positive semi-definite nature of the covariance matrix. However, because the system output consists only of individual degrees of freedom results (each row of the $\mathbf{C}_{\text{a}}$ has a single nonzero value), only the diagonal terms of the covariance matrix are used. Because the diagonal terms are always positive, the result is always a positive real number. Additional details about the stochastic dynamic sensitivity for other objectives can be found in Gomez and Spencer [36].

3.3. Implementation details

Implementation of the topology optimization procedure follows the form outlined below. For a given design domain, the problem is first idealized into a representative set of loading and structural parameters, which serve as inputs to the optimization routine. Then, the following steps are performed:

- **Initialize**: Any quantities used by the optimization routine that are constant throughout the process can be computed outside of the iterative loop to save computation time. This initialization includes building and balanced reduction of the loading system if it has not been computed previously, as well as the filter matrix and sets of indices that map individual elements to corresponding rows and columns of the global matrices for efficient assembly operations. Also, the initial values of the design variables are established.
- **Linear Static and Stochastic Dynamic Analysis**: Using the design variables, build the structural system and augmented state space matrices. Then solve for the static response to the mean load and the stochastic dynamic response variance using the stationary Lyapunov equation.
- **Compute Sensitivities**: Use the adjoint approach to solve for the sensitivities of the static mean response and the stochastic dynamic response.
- **Update Design Variables**: Using the sensitivities, compute the new set of design variable values. This updating step requires a procedure that can handle both positive and negative values, here the Generalized Optimality Criteria Method (GOCM) [37] is used.
- **Convergence**: If the iterations are no longer changing design variable values or improving the objective function, results have converged.

To facilitate the optimization routine, while maintaining an accurate representation of the bridge structure, a number of additional features need to be considered, as discussed below.

3.3.1. Lumped masses

For the structures considered here, the optimization generates a 2D idealization of the bridge superstructure. This approximation does not include components in the out of plane dimension, required to distribute load from the vehicles to the superstructure, i.e., the floor system. The mass of the floor system components (floorbeams, stringers, concrete deck, etc.) as well as the mass from other nonstructural components (railings, curbs, barriers, wearing surfaces, utilities, etc.) is accounted for using discrete lumped masses at the nodes designated as floorbeam locations. These masses are independent of the density design variables and are added to the mass matrix of the element mesh in each iteration of the optimization.

3.3.2. Guyan reduction

To improve computational efficiency, the size of the structural matrices can be reduced via Guyan reduction [38], which has been demonstrated in topology optimization of buildings [29]. Generally, a large portion of a bridge structure's mass is within the concrete deck. As shown in [39], typical steel weight for an arch type bridge superstructure can be estimated by

$$wt = 0.027L + 2.3962 \tag{20}$$

where wt represents the weight of steel per road surface area in units of kN/m^2 given a span length of L (m). For a 200m span, wt is $7.8\,\text{kN/m}^2$, assuming the same structure has a concrete deck of thickness 0.2m and weight density of 23.6kN/m^3, the deck weight is $4.7\,\text{kN/m}^2$, resulting in a weight distribution of 62% superstructure and 38% deck. If additional dead loads applied directly to the deck are considered (for example nonstructural elements, wearing surfaces, utilities, etc.) the percentage of the weight directly at the deck level is even higher. As a result, the inertial forces associated with the floorbeam degrees of freedom are selected as the retained DOF; the validity of the Guyan reduction for bridge structures is shown in the first numerical example. For more information on the use of the Guyan reduction in topology optimization, see Gomez et al. [29].

3.3.3. Passive region

To ensure stability of the optimization process, the elements in the domain corresponding to the road elevation are enforced as a passive solid region, typically consisting of one or more rows of elements. That is, this region of elements is not part of the design domain and is always considered to have a unit element density. This approach prevents the

load from being applied on a very low stiffness region. From a practical perspective, this row of elements is akin to a bottom chord of a truss, or the tie of a tied arch bridge. While this passive solid may not be needed for the vertical displacement objectives considered here, it provides a lateral load path for longitudinal demands from vehicle braking and seismic loading.

3.3.4. Penalty & filter

To push the topology toward a nearly binary result, a modified SIMP material penalization scheme is used as recommended by Gomez and Spencer [36] where both the material modulus, E, and mass density, ρ, are functions of the element design density, z.

$$E(z) = [\epsilon + (1-\epsilon)z^p]E_0$$

$$\rho(z) = \begin{cases} z^q\rho_0 & \text{if } z \geq 0.1 \\ 10^{p+3-q}z^{p+3}\rho_0 & \text{if } z < 0.1 \end{cases} \tag{21}$$

where E_0 and ρ_0 are Young's modulus and density for the solid material, ϵ is a small but nonzero value, and p and q are penalization factors. SIMP is implemented in a continuation approach along with a density filter to avoid a checkerboard type solution as recommended by Bendsøe and Sigmund [34]. To achieve a nearly binary final topology, the filtering scheme is changed to a sensitivity filter during the last step of the penalty continuation. Note that many variants of the sensitivity filter have been explored [40]. Here, a modified version that eliminates the density weighting in the denominator is used, shown as equation (16) of Sigmund [40] without ρ_e in the denominator.

3.3.5. Enforced symmetry

For traffic in a single direction, the loading and the resulting topology will not be symmetric; thus, the system cannot be evaluated using half of the domain, as typically done to reduce the size of static topology optimization problems. If the applied loading considers symmetric lanes of traffic, that is an equal number of lanes in each travel direction, then the loading will be symmetric, as well as the topology. Nonetheless, we would like to have a symmetric structure, even at some modest cost to the objective function; therefore, symmetry is enforced by modifying the sensitivity matrix to be symmetric.

3.3.6. Parameter Update scheme

The process of updating design variables given the sensitivities of the objective and constraint can be achieved in a number of ways. The method of moving asymptotes MMA [41] is popular and highly cited. More recently developed alternatives include ZPR [42], or the Generalized Optimality Criteria Method (GOCM) [37]. The GOCM method is selected here for its simplicity and effectiveness. This approach separates the positive and negative portions of the sensitivity to enable an updating scheme that is nearly as straightforward as the original optimality criteria approach.

3.3.7. Parallelization

One of the most time-consuming portions of the procedure described herein is the calculation of element sensitivities per Eq. (17). However, because each element's sensitivity is independent of other elements, these can be computed in parallel, substantially reducing the total time required, especially on computers that support a high number of parallel processes.

Using the methodology and implementation details described here, the following section demonstrates the efficacy of this topology optimization approach with a numerical example.

4. Numerical studies

In this section, the proposed optimization procedure is demonstrated. Because the topology optimization process tends to produce arch-like or truss-like structures, the target span length considered here is selected based on typical spans for these bridge types, which is in the range of 120m to 310m for arch bridges and 120m to 370m for truss bridges [43]. For this example, a pin supported bridge with a 200m span is considered. The design domain represents the bridge superstructure, but not the floor system. As such, the moving loads are assumed to be carried by the floor system (deck, stringers and floorbeams) to the superstructure at discrete intervals corresponding to the floorbeam locations. The example utilizes a steel superstructure, where the amount of material available for the design is estimated based on the statistics of existing truss and arch bridges [39] as a function of the span and road surface area. Assuming a 200m span arch bridge, the corresponding weight of the steel in the superstructure is 7.8kN/m^2 of road surface. For a two-lane bridge, assuming 10m roadway width, 200m^3 of steel would be available for the optimization. A deck thickness of 0.2m is assumed in computing the lumped masses of the deck. A loading system target frequency of 5 Hz (i.e., the bandwidth over which the Padé approximation is accurate) was selected here after confirming the use of higher target frequencies produced nearly identical results. A full list of loading and structural parameters selected for the studies in this section are listed in Table 1.

Table 1
Parameters considered in the example.

Structural Parameters		
Span	L	200m
Height	H	$L/2 = 100\,\text{m}$
Floobeam spacing		$L/10 = 20\text{m}$
Elastic modulus	E_0	200e9 Pa
Superstructure mass density	ρ_0	7850kg/m^3
Poisson's Ratio	ν	0.3
Rayleigh Damping (1st & 3rd Mode)	ζ	1%
Deck mass density	ρ_{deck}	2400kg/m^3
Superstructure weight		7.8kN/m^2
Deck width		11.4m
Road width		10m
Deck thickness		0.2m
Loading Parameters		
Loading system frequency target		5 Hz
Loading discretization	Δ_x	$L/512$
Vehicle Arrival Rate (per lane)	λ	1 load/s
Mean load magnitude	μ_A	89.0kN
Variance of load magnitude	σ_A^2	659.5kN^2
Load magnitude range	$A_{max} - A_{min}$	89.0kN
Load velocity	v	26.0m/s
Mean load (per lane)	$\mu_A\lambda/v$	3.4kN/m
Lanes		2(in opposite directions)
Optimization Parameters		
Mesh		200×100
Element size		$1\,\text{m} \times 1\,\text{m}$
Volume fraction		0.2
Penalty	(p, q)	$(1.25 : 0.25 : 4.00, 1.0)$
Filter radius		2 m

Before demonstrating the topology optimization behavior, two preliminary studies are presented. Section 4.1 verifies the effectiveness of the Guyan reduction for the structural system, including the associated sensitivities. Then, Section 4.2 presents a loading system discretization refinement study. After confirming the efficacy of the proposed approach, optimal topologies for different objectives and traffic parameters are explored.

4.1. Verification of Guyan reduction

To validate the adequacy of the proposed Guyan reduction approximation, a preliminary optimization was performed on a coarse mesh model of 100x50 elements to generate a representative topology. Then, the Hankel singular values [44] were computed and for both the full and

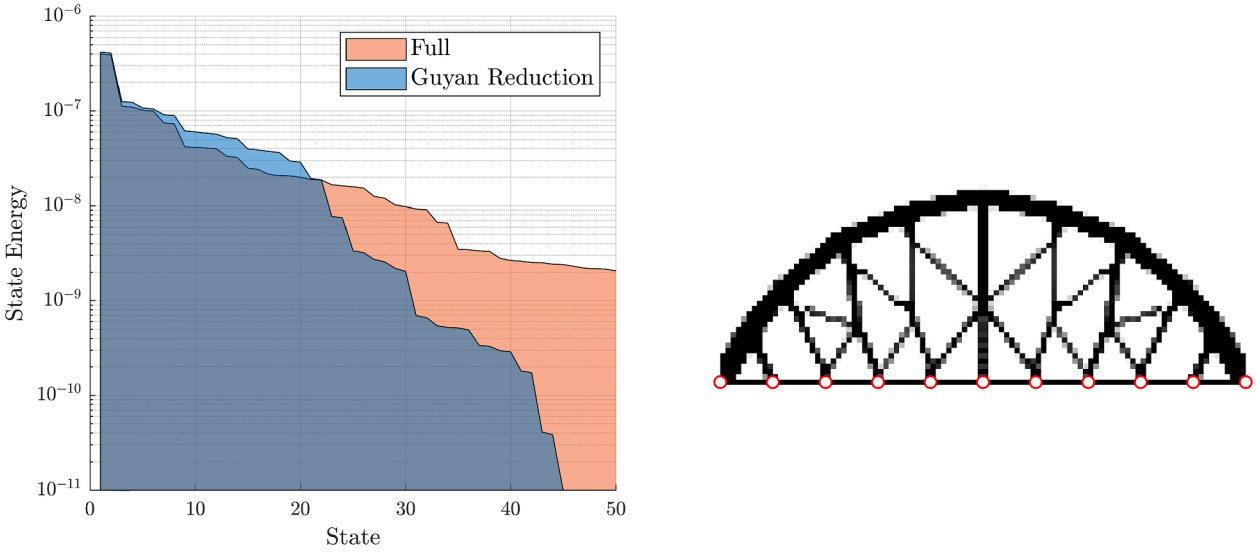

Fig. 5. Left: plot of Hankel singular values of the full and reduced structural systems, right: topology with retained degrees of freedom indicated.

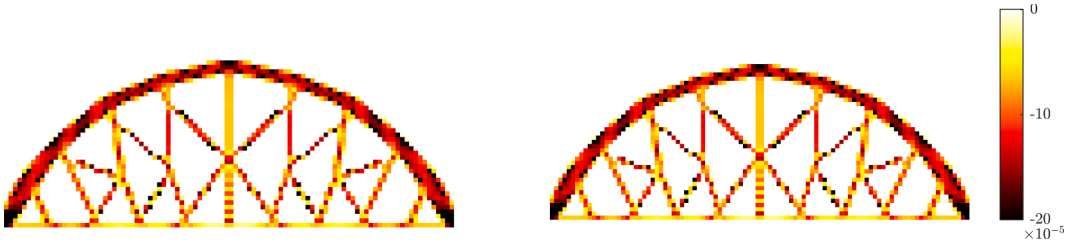

Fig. 6. Comparison of sensitivities computed using full matrices (left) and Guyan reduced matrices (right). Maximum difference between the two is 1.7e-6 (Note that the sensitivity of the corner elements, near the boundary condition, is 30 times higher than the adjacent elements, the color scale used here is adjusted to highlight the range of the majority of the domain.).

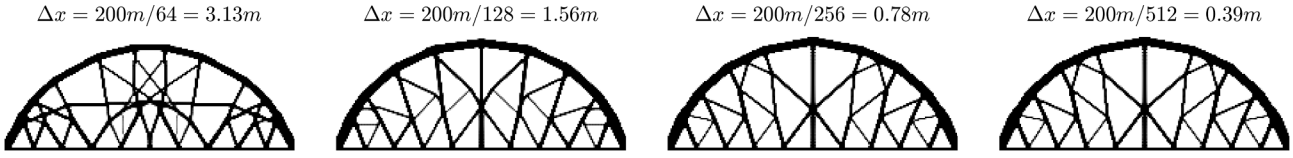

Fig. 7. Loading system discretization refinement study.

Guyan reduced structural systems of this topology, these are compared in Fig. 5. The reduced model has two retained degrees of freedom at each of the 11 floorbeam nodes, resulting in a system with a total of 44 singular values. The good agreement in the first 20 high energy states between the full and reduced systems confirms that the input–output behavior is retained in the reduction process. Evaluating the objective function, $J_{\mu k\sigma} = J_{\text{som}}(z) + 3J_{\text{sosd}}(z)$, using the full and the Guyan reduced systems produces results with only 0.002% difference. As a validation of

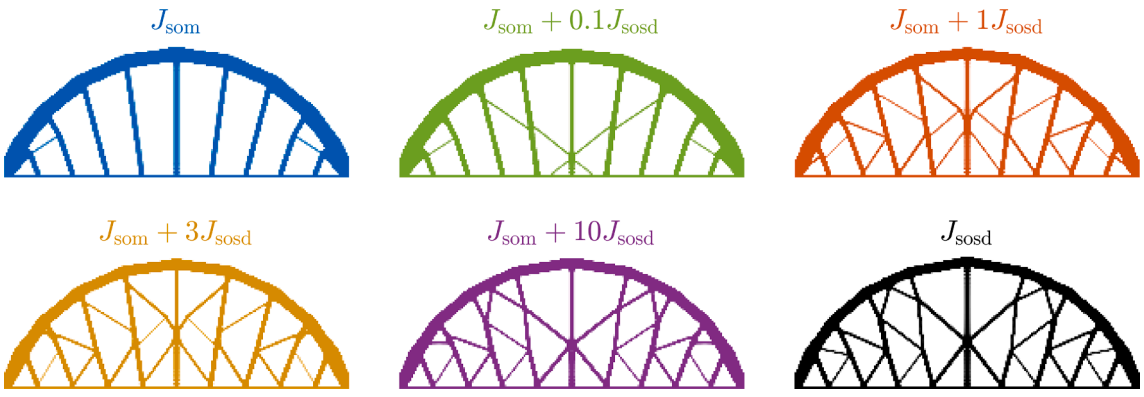

Fig. 8. Optimal topology for various objective functions.

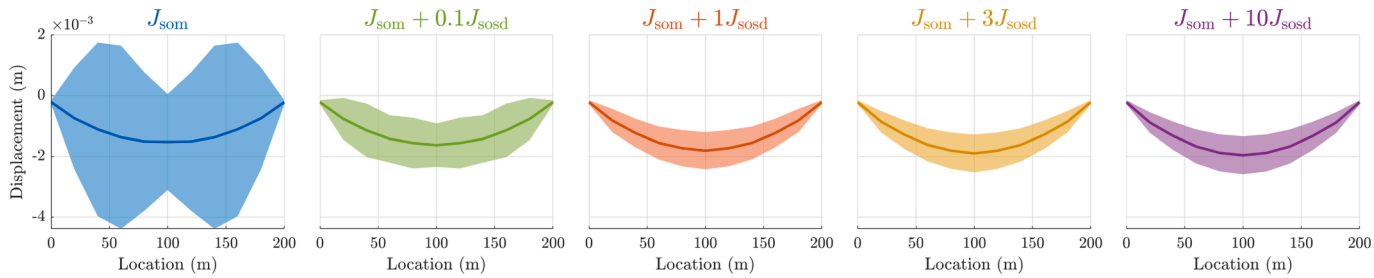

Fig. 9. Comparison of floorbeam displacement for topologies from various objective functions.

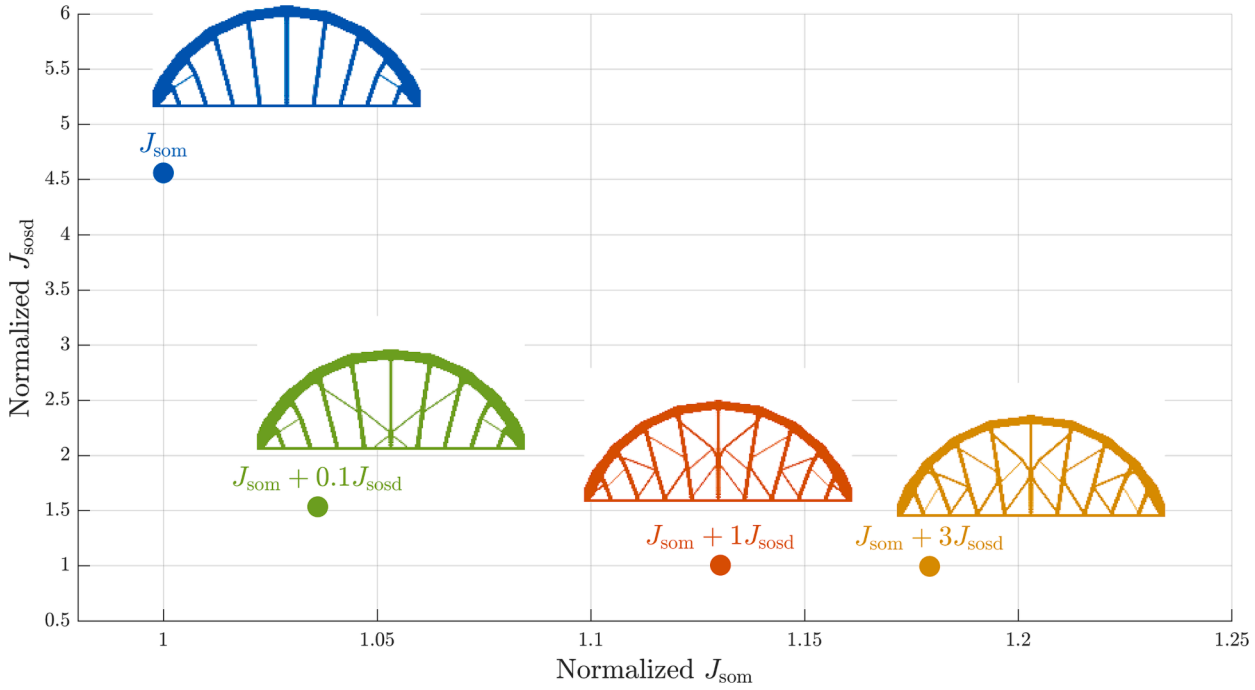

Fig. 10. Pareto-Optimal front between minimizing mean and variance of displacement.

the sensitivity calculation, the adjoint sensitivity for the same objective function is computed with and without Guyan reduction and compared in Fig. 6. These results indicate that the Guyan reduction is an effective tool for reducing the computational burden in topology optimization.

4.2. Loading discretization refinement

As discussed in [30] and Section 2, the refinement of the loading discretization affects the accuracy of the stochastic dynamic responses computed using Eq. (6). To ensure an adequate discretization, loading system models with successively finer discretizations are generated using the proposed compounding method and used for the separate topology optimizations. The resulting topologies optimized for the sum of standard deviation objective function using different loading system discretizations are shown in Fig. 7. The topology resulting from 256 and 512 loading discretization points is nearly identical, indicating convergence. Note that the compounding method for generating the loading systems discussed in Section 2.3 was required to achieve the finer discretizations used here. The remainder of this example utilizes a loading system discretization of 512 points.

4.3. Parametric study of optimal bridge topologies

Having validated the use of the Guyan reduction and the loading system discretization, the proposed topology optimization method is now used to study several model parameters. First, the topology resulting from different levels of specified probabilistic responses are compared; then, the effects of various traffic parameters on the optimal topology are investigated.

As the intent of this work is to enable optimization with respect to different levels of the probabilistic responses, a study comparing the influence of the k in the $J_{\mu k\sigma}$ objective function is performed. Using the parameters shown in Table 1, the optimal topologies for the objectives J_{som}, $J_{\mu k\sigma}$ with $k \in [0.1, 1, 3, 10]$ along with J_{sosd} are generated. The resulting topologies are compared in Fig. 8, which shows that an increase in k tends to reallocate material from the main arch to the diagonal braces. This distribution of material can be interpreted as the main arch reducing the mean response, and the diagonal braces reducing the irregularity of response. Therefore, a higher value of k places more emphasis on the uniformity of response, resulting in a more interconnected structure.

To compare the stochastic responses achieved by each of these solutions, Fig. 9 plots the mean displacement along with a shaded region representing one standard deviation above and below the mean at the floorbeam nodes. Note that the J_{som} topology shows the lowest mean response, but also has the highest variability; this high variability is the result of a lack of bracing between the vertical hangers, which also has been observed in Beghini et. al.[45]. Fig. 10 presents these results as a Pareto optimal front in terms of minimizing mean J_{som} and the variance of displacement J_{sosd}, which indicates that considering a small portion of

Fig. 11. Optimal topologies for J_{sosd} at different vehicle speeds.

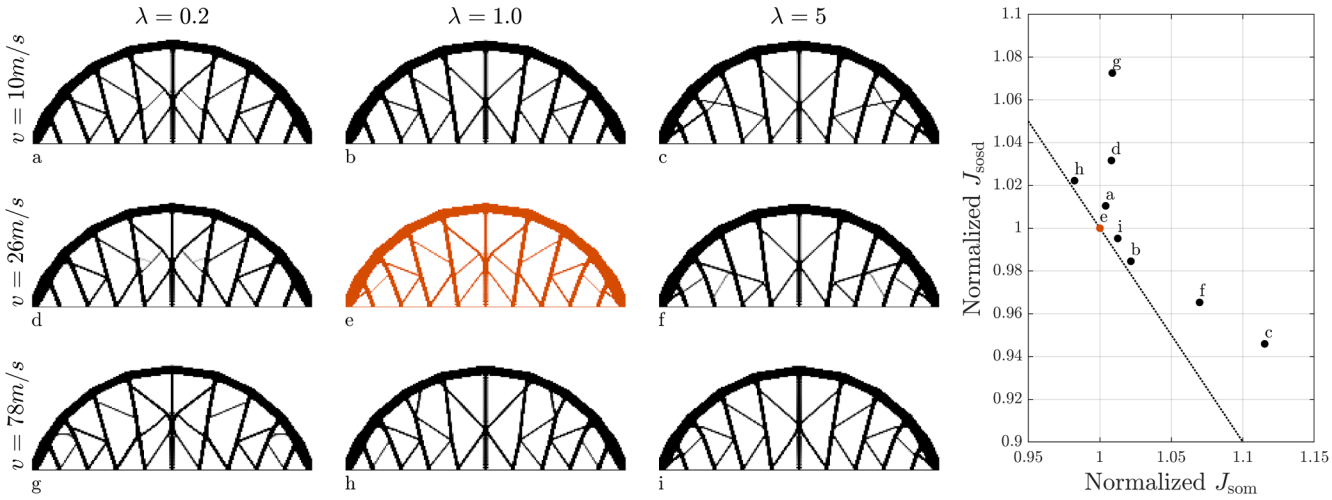

Fig. 12. Left: Optimal topologies for $J_{\mu k\sigma}$ with $k = 1$ for different speeds and arrival rates, right: comparison of performance of each topology at $v = 26m/s$ and $\lambda = 1.0$, dotted line indicates combinations of mean and standard deviation with equivalent objective to topology e.

the stochastic variability of the response in the objective function substantially improves the total response at only a small cost to the mean response.

Next, the effect of the traffic parameters, v (the speed of the vehicles) and arrival rate λ (number of vehicles entering the bridge in a given time), are investigated. Both parameters play a role in the static mean and stochastic dynamic load components, however, in different ways. The moving load speed in the complex exponential of the stochastic dynamic load, Eq. (7), affects the loading system filter, while the arrival rate only affects the PSD magnitude. As a result, changes in the speed affect the topology optimized for just the stochastic dynamic component of loading, while changes in the arrival rate do not. Optimal topologies for the J_{sosd} objective at different speeds are shown in Fig. 11. While the arrangement of diagonal members is slightly different for different speeds, the overall trends of interconnected hangers are very similar. Both the speed and arrival rate affect the magnitude of mean loading, but it is always a uniformly distributed load, so optimizing for the mean load effect at any speed or arrival rate will produce the same topology.

In contrast, when considering the $J_{\mu k\sigma}$ objective function (i.e., the total response as a combination of mean and standard deviation), the different magnitudes of these two components result in different topologies, as shown in Fig. 12. If the arrival rate is held constant, an increase in speed results in fewer loads on the span at any instant in time, which can be interpreted as more irregularity in the loading. The resulting topology tends to shift material from the main arch toward more diagonal bracing components for higher speed traffic, as seen when comparing Fig. 12b and 12h. Generally, the optimal topologies for different vehicle speeds are relatively similar, indicating a somewhat robust solution. A similar effect is seen when holding the vehicle speed constant and changing the arrival rate. As the arrival rate increases, more loads are on the span at any given time, resulting in a slightly more uniform load, and fewer diagonals in the topology. Likewise, a lower arrival rate implies fewer loads on the span at a given time, which results in slightly more diagonal components in the optimal topology as seen when comparing Fig. 12a and 12c. Fig. 12 also compares the performance of multiple topologies when evaluated at non-optimal speeds and arrival rates, and generally, their performance is within about 10% of the optimal topology, indicating a robustness of the optimal design, that good performance is achieved, even for loading other than that considered in the optimization.

In summary, lower arrival rates or higher traffic speeds result in structures with more interconnected hangers, as opposed to higher arrival rates and lower traffic speeds which allocate more material to the main arch.

5. Conclusions

This paper presented an approach for topology optimization of bridge structures subjected to random moving traffic loads. This approach resolves the computational barriers with the continuous filtered white noise representation of traffic loading developed by Golecki et. al. [30], and implements a stochastic topology optimization objective function that enables direct minimization of response extremes, which represents the probabilistic design intent to achieve adequate levels of performance under the loading uncertainties in typical bridges. A new compact loading system formulation referred to here as the compounding method is proposed which enables the generation and balanced reduction of loading systems large enough to show convergence of topology with further refinement. The topology optimization framework is achieved using an adjoint formulation to compute the gradients of the objective function, which considers both the sum of nodal response means and standard deviations at node locations that correspond to points where the bridge floor system is supported by the superstructure. This new probabilistic objective function enables determining a reliability-based optimal topology by representing the probabilistic design intent of targeting the upper tail of the random traffic loading.

Results show that accounting for the randomness of traffic can significantly improve the total response compared to optimizing for just the mean load, as is common in the literature. Because the static mean

load is a constant and uniformly distributed load, determining the optimal configuration is an established benchmark problem [46,47]. However, a topology optimized for the mean performs poorly in terms of the stochastic dynamic responses, because of the lack of bracing between vertical hangers. When the optimization objective is given in terms of the extreme responses (i.e., as a combination of the mean and some multiple of the standard deviation of responses), small changes in the topology result in substantial improvements in the variability of the stochastic bridge response at a small cost to the mean response. Additionally, the optimal topology is dependent on the traffic speed and arrival rate, with lower speeds and higher arrival rates resulting in more material in the diagonals and hangers. However, even with these dependencies, the performance achieved by the structure optimized for stochastic moving loads, when evaluated for non-optimal loading parameters is still very good, indicating a robust solution.

The novelty of this research lies in the fact that the stochastic dynamic nature of traffic loading can be incorporated into a topology optimization framework to yield optimal bridge structures. This approach is enabled by the new compact formulation of the continuous representation of random traffic loading, combined with the proposed objective function that minimizes the extreme structural response, paralleling the reliability-based design intention that targets the upper tail of the probabilistic responses.

CRediT authorship contribution statement

Thomas Golecki: Conceptualization, Methodology, Software, Writing – original draft, Writing – review & editing, Visualization. **Fernando Gomez:** Conceptualization, Writing – review & editing. **Juan Carrion:** Conceptualization, Writing – review & editing. **Billie F. Spencer:** Conceptualization, Writing – review & editing.

Declaration of Competing Interest

The authors declare that they have no known competing financial interests or personal relationships that could have appeared to influence the work reported in this paper.

Data availability

Data will be made available on request.

Acknowledgements

This work made use of the Illinois Campus Cluster, a computing resource that is operated by the Illinois Campus Cluster Program (ICCP) in conjunction with the National Center for Supercomputing Applications (NCSA) and which is supported by funds from the University of Illinois at Urbana-Champaign.

Appendix A. – Efficient loading system generation

This appendix describes the implementation of the compounding method of system assembly discussed in Section 2.3. For a given domain, a spatial discretization of loading, Δx, and a velocity, v, are used to compute the time delays needed in the assembled loading system. The input to the assembled system is a white noise, and the first output is a delayed version of that input, where the time delay is equal to the time required to travel the distance Δx at velocity v. Each additional output extends this delay by an additional $\Delta x/v$, corresponding to the remaining discrete locations along the span. The first step in generating the compact form of the assembled loading system is creating a base system, $\boldsymbol{d}_2$, which accounts for the first two sequential delays. The subsystems with the first two incremental delays are assembled in parallel using Eq. (8) where $d(\Delta x/v)$ represents a single-input, single-output (SISO) state space system of a time delay of $\Delta x/v$ generated as a Padé approximant. The corresponding block diagram is shown in Fig. 2. For the first compounding iteration, $i = 1$ in Eq. (9), the assembly consists of the base system in parallel with a delayed base system, where the delayed base system is represented as a series combination of a SISO delay system and the base system. The result is four outputs with sequentially increasing delays given by

$$\boldsymbol{d}_4 = \begin{bmatrix} \begin{bmatrix} d(\Delta x/v) \\ d(2\Delta x/v) \end{bmatrix} \\ d(2\Delta x/v)^* \begin{bmatrix} d(\Delta x/v) \\ d(2\Delta x/v) \end{bmatrix} \end{bmatrix} \tag{22}$$

$$\boldsymbol{d}_8 = \begin{bmatrix} \begin{bmatrix} \begin{bmatrix} d(\Delta x/v) \\ d(2\Delta x/v) \end{bmatrix} \\ d(2\Delta x/v)^* \begin{bmatrix} d(\Delta x/v) \\ d(2\Delta x/v) \end{bmatrix} \end{bmatrix} \\ d(4\Delta x/v)^* \begin{bmatrix} \begin{bmatrix} d(\Delta x/v) \\ d(2\Delta x/v) \end{bmatrix} \\ d(2\Delta x/v)^* \begin{bmatrix} d(\Delta x/v) \\ d(2\Delta x/v) \end{bmatrix} \end{bmatrix} \end{bmatrix} \tag{23}$$

where * represents the series combination of two systems. The corresponding block diagram is shown in Fig. 13.

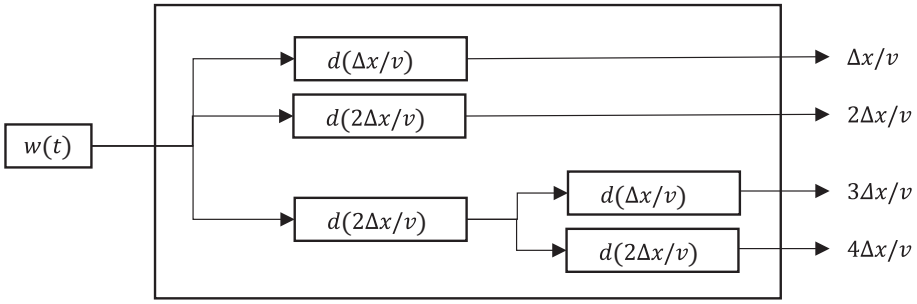

Fig. 13. Block diagram of assembled loading system, d_4, with four outputs (outputs are labeled with their time delay).

For the second compounding iteration, $i = 2$ in Eq. (9), the procedure is repeated. The result is eight outputs with sequentially increasing delays. The corresponding block diagram is shown in Fig. 14.

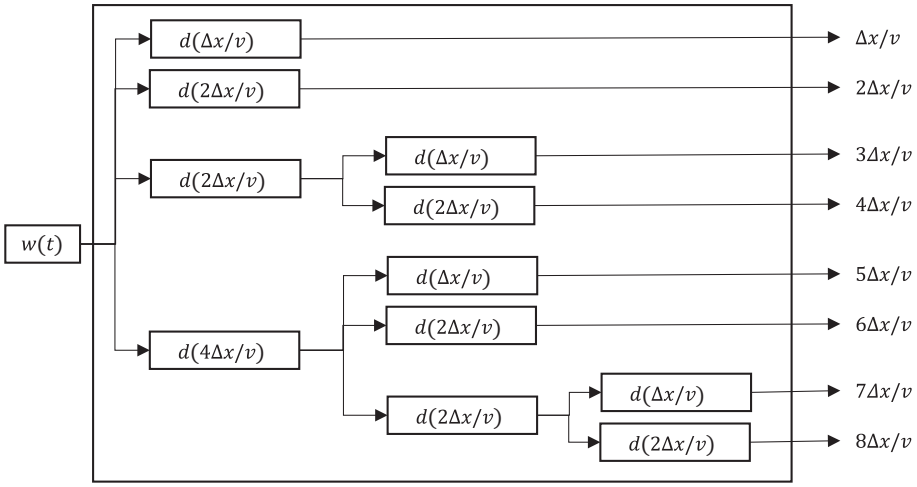

Fig. 14. Block diagram of assembled loading system, d_8, with eight outputs (outputs are labeled with their time delay).

This assembly procedure is repeated as many times as necessary to generate the required number and timing of output delays.

References

[1] National Bridge Inventory, Federal Highway Administration 2020. https://www.fhwa.dot.gov/bridge/nbi.cfm (accessed March 21, 2022).

[2] Novotny AA, Lopes CG, Santos RB. Topological derivative-based topology optimization of structures subject to self-weight loading. Struct Multidiscip Optim 2021:1–9. https://doi.org/10.1007/s00158-020-02780-4.

[3] Bruyneel M, Duysinx P. Note on topology optimization of continuum structures including self-weight. Struct Multidiscip Optim 2005;29:245–56. https://doi.org/10.1007/s00158-004-0484-y.

[4] Zhang S, Li H, Huang Y. An improved multi-objective topology optimization model based on SIMP method for continuum structures including self-weight. Struct Multidiscip Optim 2021;63:211–30. https://doi.org/10.1007/S00158-020-02685-2/FIGURES/26.

[5] Rahmatalla S, Swan CC. Form finding of sparse structures with continuum topology optimization. J Struct Eng 2003;129:1707–16. https://doi.org/10.1061/(ASCE)0733-9445(2003)129:12(1707).

[6] Weldeyesus AG, Gondzio J, He L, Gilbert M, Shepherd P, Tyas A. Truss geometry and topology optimization with global stability constraints. Struct Multidiscip Optim 2020;62:1721–37. https://doi.org/10.1007/S00158-020-02634-Z.

[7] Oberndorfer JM, Achtzlger W, Hiirnlein HREM. Two approaches for truss topology optimization: a comparison for practical use, vol. 11. Springer-Verlag; 1996.

[8] Liu S, Qiao H, Liu S, Qiao H. Topology optimization of continuum structures with different tensile and compressive properties in bridge layout design. Struct Multidiscip Optim 2011;43:369–80. https://doi.org/10.1007/s00158-010-0567-x.

[9] Zhang X, Ramos AS, Paulino GH. Material nonlinear topology optimization using the ground structure method with a discrete filtering scheme. Struct Multidiscip Optim 2017;55:2045–72. https://doi.org/10.1007/S00158-016-1627-7/FIGURES/21.

[10] Li Y, Lai Y, Lu G, Yan F, Wei P, Xie YM. Innovative design of long-span steel-concrete composite bridge using multi-material topology optimization. Eng Struct 2022;269:114838. https://doi.org/10.1016/J.ENGSTRUCT.2022.114838.

[11] Fairclough HE, He L, Pritchard TJ, Gilbert M. LayOpt: an educational web-app for truss layout optimization. Struct Multidiscip Optim 2021;64:2805–23. https://doi.org/10.1007/S00158-021-03009-8.

[12] Guan H, Chen YJ, Loo YC, Xie YM, Steven GP. Bridge topology optimisation with stress, displacement and frequency constraints. Comput Struct 2003;81:131–45. https://doi.org/10.1016/S0045-7949(02)00440-6.

[13] Smarslik M, Ahrens MA, Mark P. Toward holistic tension- or compression-biased structural designs using topology optimization. Eng Struct 2019;199:109632. https://doi.org/10.1016/J.ENGSTRUCT.2019.109632.

[14] Fairclough HE, Gilbert M, Pichugin AV, Tyas A, Firth I. Theoretically optimal forms for very long-span bridges under gravity loading. Proc R Soc A Math Phys Eng Sci 2018;474. https://doi.org/10.1098/RSPA.2017.0726.

[15] Amir O, Mass Y. Topology optimization for staged construction. Struct Multidiscip Optim 2018;57:1679–94. https://doi.org/10.1007/S00158-017-1837-7/FIGURES/11.

[16] Dapogny C, Faure A, Michailidis G, Allaire G, Couvelas A, Estevez R. Geometric constraints for shape and topology optimization in architectural design. Comput Mech 2017;59:933–65. https://doi.org/10.1007/S00466-017-1383-6/FIGURES/32.

[17] He Y, Cai K, Zhao ZL, Xie YM. Stochastic approaches to generating diverse and competitive structural designs in topology optimization. Finite Elem Anal Des 2020;173:103399. https://doi.org/10.1016/J.FINEL.2020.103399.

[18] Xie YM, Zuo ZH, Huang X, Black T, Felicetti P. Application of topological optimisation technology to bridge design. Struct Eng Int 2018;24:185–91. https://doi.org/10.2749/101686614X13830790993366.

[19] Guest JK, Igusa T. Structural optimization under uncertain loads and nodal locations. Comput Methods Appl Mech Eng 2008;198:116–24. https://doi.org/10.1016/j.cma.2008.04.009.

[20] Dunning PD, Kim HA. Robust topology optimization: Minimization of expected and variance of compliance. AIAA J 2013;51:2656–64. https://doi.org/10.2514/1.J052183.

[21] Jeong S, Seong HK, Kim CW, Yoo J. Structural design considering the uncertainty of load positions using the phase field design method. Finite Elem Anal Des 2019;161:1–15. https://doi.org/10.1016/j.finel.2019.04.002.

[22] Zhang XS, de Sturler E, Paulino GH. Stochastic sampling for deterministic structural topology optimization with many load cases: density-based and ground structure approaches. Comput Methods Appl Mech Eng 2017;325:463–87. https://doi.org/10.1016/j.cma.2017.06.035.
[23] Chen S, Chen W, Lee S. Level set based robust shape and topology optimization under random field uncertainties. Struct Multidiscip Optim 2010;41:507–24. https://doi.org/10.1007/s00158-009-0449-2.
[24] Zhao J, Wang C. Robust structural topology optimization under random field loading uncertainty. Struct Multidiscip Optim 2014;50:517–22. https://doi.org/10.1007/s00158-014-1119-6.
[25] Deng J, Chen W. Concurrent topology optimization of multiscale structures with multiple porous materials under random field loading uncertainty. Struct Multidiscip Optim 2017;56:1–19. https://doi.org/10.1007/s00158-017-1689-1.
[26] Cai J, Wang C, Fu Z. Robust concurrent topology optimization of multiscale structure under single or multiple uncertain load cases. Int J Numer Methods Eng 2020;121:1456–83. https://doi.org/10.1002/NME.6275.
[27] Giraldo-Londoño O, Paulino GH. PolyDyna: a Matlab implementation for topology optimization of structures subjected to dynamic loads. Struct Multidiscip Optim 2021:1–34. https://doi.org/10.1007/S00158-021-02859-6.
[28] Gomez F, Spencer BF, Carrion J. Topology optimization of buildings subjected to stochastic wind loads. Probabilistic Eng Mech 2021;64:103127. https://doi.org/10.1016/j.probengmech.2021.103127.
[29] Gomez F, Spencer BF, Carrion J. Topology optimization of buildings subjected to stochastic base excitation. Eng Struct 2020;223:111111. https://doi.org/10.1016/J.ENGSTRUCT.2020.111111.
[30] Golecki T, Gomez F, Carrion J, Spencer BF. Continuous random field representation of stochastic moving loads. Probabilistic Eng Mech 2022;68:103230. https://doi.org/10.1016/J.PROBENGMECH.2022.103230.
[31] Soong TT, Grigoriu M. Random vibration of mechanical and structural systems. Englewood Cliffs, N.J: PTR Prentice Hall,; 1993.
[32] Lam J. Model reduction of delay systems using Pade approximants. Int J Control 1993;57:377–91. https://doi.org/10.1080/00207179308934394.
[33] Qu Z-Q. Model Order Reduction Techniques: with Applications in Finite Element Analysis. London: Springer-Verlag London; 2004. https://doi.org/10.1007/978-1-4471-3827-3.
[34] Bendsøe MPM, Sigmund O. Topology Optimization: Theory, Methods, and Applications. Springer Berlin Heidelberg; 2004. https://doi.org/10.1007/978-3-662-05086-6.
[35] Choi KK, Kim NH. Structural Sensitivity Analysis and Optimization 1. Springer New York; 2005. https://doi.org/10.1007/B138709.
[36] Gomez F, Spencer BF. Topology optimization framework for structures subjected to stationary stochastic dynamic loads. Struct Multidiscip Optim 2019;59:813–33. https://doi.org/10.1007/s00158-018-2103-3.
[37] Kim NH, Dong T, Weinberg D, Dalidd J. Generalized optimality criteria method for topology optimization. Appl Sci 2021:11. https://doi.org/10.3390/app11073175.
[38] Craig RR, Kurdila AJ. Fundamentals of structural dynamics. Wiley; 2011.
[39] Toma S. Weight distributions of highway steel bridges. Bridg Eng Handb, CRC Press 2014:495–516. https://doi.org/10.1201/B15616-25.
[40] Sigmund O. Morphology-based black and white filters for topology optimization. Struct Multidiscip Optim 2007;33:401–24. https://doi.org/10.1007/s00158-006-0087-x.
[41] Svanberg K. The method of moving asymptotes - a new method for structural optimization. Int J Numer Methods Eng 1987;24:359–73. https://doi.org/10.1002/nme.1620240207.
[42] Zhang XS, Paulino GH, Ramos AS. Multi-material topology optimization with multiple volume constraints: a general approach applied to ground structures with material nonlinearity. Struct Multidiscip Optim 2018;57:161–82. https://doi.org/10.1007/S00158-017-1768-3.
[43] Martin BT. Highway bridges. Innov Bridg Des Handb Constr Rehabil Maint, Butterworth-Heinemann 2016:483–508. https://doi.org/10.1016/B978-0-12-800058-8.00018-9.
[44] Antoulas AC. Approximation of large-scale dynamical systems. Soc Ind Appl Mathematics 2005. https://doi.org/10.1137/1.9780898718713.
[45] Beghini LL, Carrion J, Beghini A, Mazurek A, Baker WF, Carrion J, et al. Structural optimization using graphic statics. Struct Multidiscip Optim 2014;49:351–66. https://doi.org/10.1007/s00158-013-1002-x.
[46] Beghini A, Beghini LL, Baker WF. On the layout of a least weight single span structure with uniform load. Struct Multidiscip Optim 2014;50:49–64. https://doi.org/10.1007/s00158-013-1030-6.
[47] Hemp WS. Michell framework for uniform load between fixed supports. Eng Optim 1974;1:61–9. https://doi.org/10.1080/03052157408960577.